

Emergence of evolutionarily stable communities through eco-evolutionary tunnelling

Seyfullah Enes Kotil and Kalin Vetsigian*

Ecological and evolutionary dynamics of communities are inexorably intertwined. The ecological state determines the fate of newly arising mutants, and mutations that increase in frequency can reshape the ecological dynamics. Evolutionary game theory and its extensions within adaptive dynamics have been the mathematical frameworks for understanding this interplay, leading to notions such as evolutionarily stable states (ESS) in which no mutations are favoured, and evolutionary branching points near which the population diversifies. A central assumption behind these theoretical treatments has been that mutations are rare so that the ecological dynamics has time to equilibrate after every mutation. A fundamental question is whether qualitatively new phenomena can arise when mutations are frequent. Here, we describe an adaptive diversification process that robustly leads to complex ESS, despite the fact that such communities are unreachable through a step-by-step evolutionary process. Rather, the system as a whole tunnels between collective states over a short timescale. The tunnelling rate is a sharply increasing function of the rate at which mutations arise in the population. This makes the emergence of ESS communities virtually impossible in small populations, but generic in large ones. Moreover, communities emerging through this process can spatially spread as single replication units that outcompete other communities. Overall, this work provides a qualitatively new mechanism for adaptive diversification and shows that complex structures can generically evolve even when no step-by-step evolutionary path exists.

Understanding the consequences of the feedback between ecological and evolutionary dynamics is a fundamental challenge^{1–6}, particularly in asexual microbial communities, where new strains with altered ecological interactions can readily arise through mutational events such as replication errors and horizontal gene transfer^{7–14}. In the absence of mutations, the strain abundance dynamics can be represented as a nonlinear dynamical system with fixed dimensionality determined by the number of strains^{15–18}, which allows us to understand and classify long-term community composition in terms of dynamical attractors. However, it is far less clear how to analyse the dynamics when mutations stochastically introduce new ecological dimensions and interactions^{19–22}.

Important progress was made with the advent of evolutionary game theory^{23–28}, which established the notion of evolutionarily stable states (ESSs) as long-term end-points of the eco-evolutionary dynamics. An ESS is a community that has reached an ecological attractor that cannot be invaded by any possible mutant. Therefore, an evolutionarily stable community (ESC) would persist indefinitely despite mutations. These ideas were further elaborated on through the framework of adaptive dynamics^{29–31}, which went beyond analysis of equilibria. Here, community evolution is represented as a sequence of mutational events (Fig. 1a). After every mutational event, the ecological dynamics has time to equilibrate and reach a new ecological attractor. Thus, the evolutionary dynamics consists of a series of stochastic jumps from one ecological attractor to another, and an ecological attractor can, in general, transition to many different attractors through different mutations (Fig. 1b). The space of possible strains and attractors is typically continuous, reflecting the continuous nature of phenotypes. It was recognized that some ESSs can be unreachable by evolution ('Gardens of Eden')³², and therefore the notion of evolutionary convergence was introduced to indicate ecological attractors towards which all nearby attractors evolve.

Strikingly, evolutionary stability and evolutionary convergence are independent notions that can occur in all possible combinations^{29,33}. States that are both convergent and stable are end-points of the eco-evolutionary dynamics. In contrast, ecological attractors that are evolutionarily convergent but unstable (branching points) lead to adaptive diversification events, where a lineage splits into multiple coexisting lineages. Thus, adaptive dynamics has provided tools for analysing equilibrium end-points of the eco-evolutionary dynamics and adaptive diversifications³⁴.

A fundamental limitation of the adaptive dynamics framework is the assumption that ecologically relevant mutations are rare, so that the ecological dynamics has time to equilibrate between mutations³⁰. In a sense, it is assumed that there is a separation of timescales between the ecological and evolutionary dynamics. However, even if the rate of discovery of ecologically relevant mutations is low per individual, many communities contain very large numbers of individuals. Therefore, it is quite possible that a new mutant will start invading before the transient dynamics triggered by the previous successful mutant has expired. This would be especially true if the selection coefficients of invading mutants are low, so that the transient ecological dynamics is long.

An important question, then, is whether the realistic regime of a finite mutation rate per population, rather than an infinitesimal one, can exhibit qualitatively new behaviours that fall outside the scope of adaptive dynamics. Previous work has already investigated cases where multiple mutants compete with each other (that is, clonal interference)^{35,36} or multiple mutations accumulate in the same lineage without intermediate fixation events³⁷. Such phenomena were shown to be important for determining the rate at which fitness increases in a population³⁸, the rate at which fitness valleys are crossed^{39,40} and tumorigenesis⁴¹. However, these studies assume—as is customary in population genetics—that mutants compete within

Department of Bacteriology and Wisconsin Institute for Discovery, University of Wisconsin-Madison, Madison, WI, USA.

*e-mail: kalin.vetsigian@wisc.edu

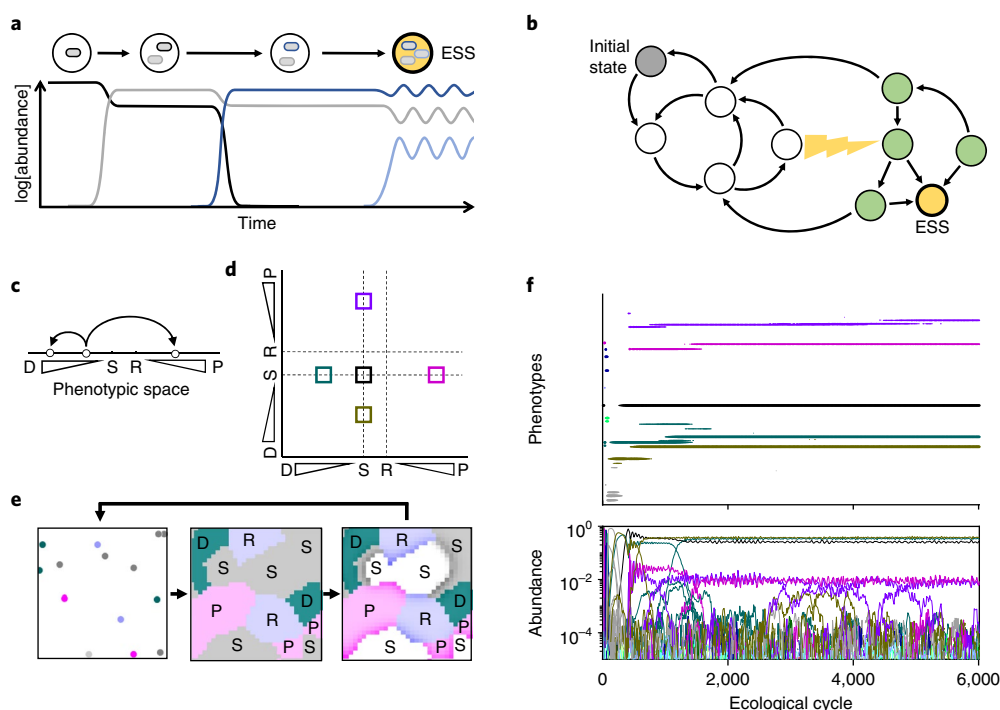


Fig. 1 | Evolution of antibiotic interactions leads to robust emergence of ESCs that are unreachable through adaptive dynamics. a, Schematic of adaptive dynamics. Mutant invasions (arrows) lead to transitions between ecologically stable communities (circles) containing one or more strains. ESS corresponds to a state from which no further transitions are possible (yellow circle). The abundances of different strains over time (coloured lines) corresponding to the transitions are also shown. **b**, A more general adaptive dynamics graph in which multiple paths are possible, and in which certain ecologically stable communities (green) are unreachable starting from an initial community (grey). However, these communities can be reached through eco-evolutionary tunnelling that falls outside the scope of adaptive dynamics (yellow lightning). **c**, In simulations, strains genetically encode different levels of antibiotic production (P) or degradation (D). They can also be sensitive to antibiotics (S) or resistant via an antibiotic efflux (R). New strains can emerge through mutations (arrows). **d**, Space of possible strain phenotypes in simulations with two antibiotics. The five-strain ESS that emerges in **f** is indicated by coloured squares. **e**, Simulations of microbial communities proceed through ecological cycles. During each cycle, spores of different strains (different colours) are scattered on a 2D plane and grow as colonies until all space is filled. Colonies then produce and degrade diffusing antibiotics according to their phenotypes. Some regions die (white), while sporulation is enhanced if neighbours are inhibited (darker colours). **f**, In a simulation with two antibiotics, a five-strain ESS robustly arises. Top, existing phenotypes (projected onto one dimension) as a function of time. Bottom, abundance of different strains over time. Different colours correspond to different phenotypic classes (Methods).

the same ecological niche and differ only in their selection coefficients. Here, we extend such investigations to the general case where the arising mutants can reshape the ecology by introducing new interactions and frequency-dependent relationships.

Recently, we computationally examined the eco-evolutionary dynamics in microbial communities in which bacteria consume a single resource in a two-dimensional (2D) environment and compete through interactions mediated by antibiotic production and degradation⁴². Each strain is characterized by its costly investment in antibiotic production or degradation with respect to each antibiotic, and mutants with different levels of antibiotic production and degradation can arise (Fig. 1c–e and Methods). We found that, for a broad range of parameters, ESCs with three strains and five strains robustly arise in simulations with one and two antibiotics, respectively, when starting with a single strain. Thus, stable communities maintained solely by antibiotic-mediated interactions can spontaneously evolve. Here, we investigate the mechanism behind these adaptive diversifications. We show that, while locally convergent, the ESCs are globally inaccessible through step-by-step adaptive dynamics, starting from simple single-strain populations (Fig. 1b). The robust emergence of these ‘forbidden’ ESCs is only possible when the timescales of the ecological and evolutionary dynamics interfere with each other through a process we term ‘eco-evolutionary tunnelling’.

Results

ESCs appear to come together all at once (Fig. 1f). To disentangle the sequence of events leading to their formation, we lowered the mutation rate per population in the hope of stretching out the assembly process over time and unambiguously separating the individual adaptive steps. We found that while lowering the mutation rate tends to dramatically delay the emergence, the stable communities still snap together on a very short timescale, and each community formation event requires multiple near-simultaneous mutant invasions (Fig. 2a). Before the transition, the system spends a lot of time in a regime of rapid turnover, in which the dominant strains are continuously outcompeted by new mutants. This regime ends abruptly with the emergence of a persistent multi-strain community that can then evolve towards the convergent ESC. This transition is stochastic, and the wait time (T) is exponentially distributed (Fig. 2b and Supplementary Figs. 1 and 2). This suggests a simple two-state representation in which the rapid turnover state is metastable and decays into the ESC state by stochastically tunnelling through a barrier with a constant probability per unit time (Fig. 2c).

Next, we investigated how the tunnelling rate (r) depends on the mutation rate (μ) and population size (N). If the community emerges step by step (Fig. 1a), we expect that, at low μN , the inverse of the mean community formation time would be simply proportional to the mutation rate per population (μN), independent of

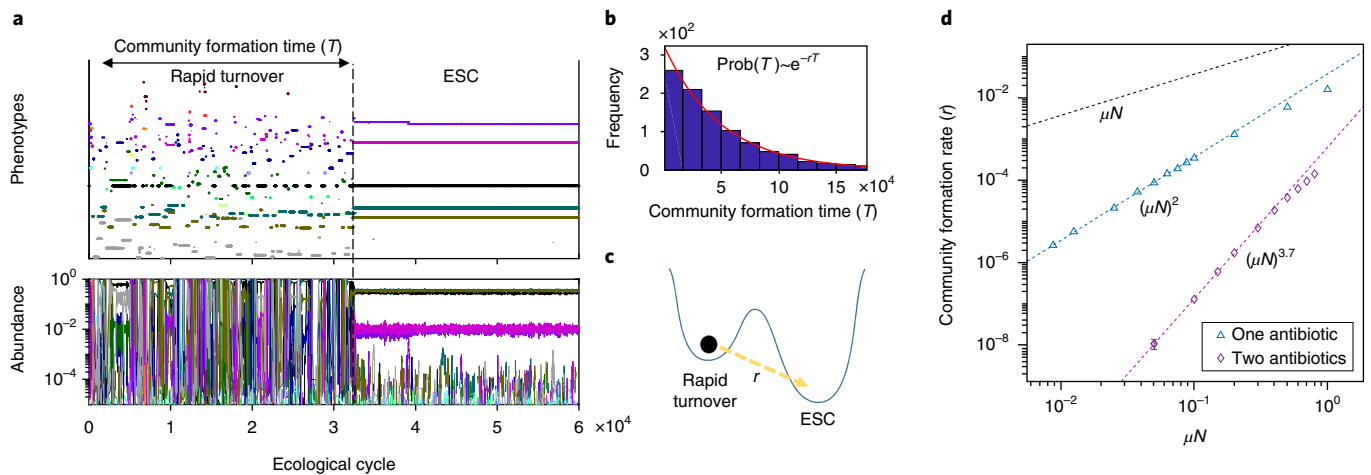


Fig. 2 | ESCs emerge abruptly through eco-evolutionary tunnelling whose rate scales superlinearly with mutation rate and population size. **a**, At lower mutation rates, the dynamics can spend a considerable time in a rapid strain turnover phase before suddenly arriving at a stable solution (ESC). **b**, The community formation time is exponentially distributed, indicating a constant probability of formation per unit time. **c**, Two-state representation of the system in which a metastable rapid turnover state decays into an ESC state by tunnelling through a barrier with a constant probability per unit time, r . **d**, The community formation rate r , as computed from thousands of replicate simulations (Supplementary Figs. 1 and 2), is shown as a function of μ at fixed N for simulations with one antibiotic (blue triangles) and two antibiotics (purple diamonds). Note the logarithmic scale on both axes. Straight lines (dashed, blue and purple) are fitted to the data to demonstrate power-law dependence at low μN . The expected slope from adaptive dynamics for $r=1/\langle T \rangle$ is shown as a reference (dashed black line). The estimation errors of r are smaller than the symbols except for the point with an error bar. By independently varying μ and N , we verified that the controlling parameter is the product μN , which is the mutation rate per population (Supplementary Fig. 3).

ecological details. This is because the rate of every adaptive dynamics transition is proportional to μN , and therefore the mean time to go through any sequence of adaptive steps scales as $(\mu N)^{-1}$ (Methods). In sharp contrast, we found that r is proportional to $(\mu N)^2$ for the three-strain community that emerges in a universe with one antibiotic, and r exhibits a complex dependence with an approximate $(\mu N)^{3.7}$ scaling for the five-strain community that emerges in a universe with two antibiotics (Fig. 2d and Supplementary Fig. 3). The superlinear dependence of r clearly demonstrates that ESC emergence cannot be understood within the context of step-by-step adaptive dynamics and, strikingly, that emergence becomes ever more efficient at high mutation rates or population sizes (a stable community is reached after fewer mutations occur in the population). Furthermore, the different scaling exponents at low μN in the two examined cases indicate that there are different classes of eco-evolutionary emergence.

Community emergence can be understood as a probabilistic escape from the rapid turnover regime. This can happen when the turnover dynamics passes through an exit window and requires a well-timed sequence of mutant invasions, which we term a high-order eco-evolutionary event (Fig. 3). The emergence of a three-strain community maintained by one antibiotic provides the simplest possible example and requires a single well-timed mutation that happens during an ongoing transition of the rapid turnover dynamics from one state to another (Fig. 3a). Given an ongoing transition, the probability (P) of such a mutation arising is proportional to $(\mu N)W$ for small P , where W is the duration of the window of opportunity. In contrast, the arrival at an exit window during rapid turnover is governed by step-by-step evolution and, therefore, the mean waiting time between visits to exit windows scales as $(\mu N)^{-1}$. In other words, the frequency (f) with which the system passes through exit windows is proportional to μN . Therefore, $r=fP \sim (\mu N)^2$, explaining our empirical finding for simulations with one antibiotic (Methods). Note that as μN is increased, the tunnelling probability P will eventually start saturating, which will lead to a decrease in the apparent scaling exponent. The onset of such a tunnel saturation is indeed apparent in Fig. 2d at the highest μN point.

Simulations with two antibiotics provide a more general example in which multiple well-timed mutant invasions are required, and in which a community can emerge through multiple possible pathways (Fig. 3b,c and Supplementary Figs. 4 and 5). The pathway in Fig. 3b shows that two higher-order eco-evolutionary events, separated by a stable stepping-stone community, can act in combination to enable complex community formation. A simple analysis suggests that each higher-order event increases the scaling exponent of r based on the number of well-timed mutations, while the number of adaptive dynamics steps does not affect the scaling (Methods). This analysis predicts $r \sim (\mu N)^4$, which is close but not identical to the observed exponent of about 3.7. The discrepancy is probably due to the fact that we have not reached the true asymptotic behaviour at low μN .

Strikingly, the pathway that was overall most frequently utilized in our simulations went directly from one strain to five strains, without any ecologically stable intermediates (Fig. 3c). This implies $r \sim (\mu N)^5$, making the dominance of this pathway puzzling. At the lowest μN , we could reach a regime where the stepping-stone pathway from Fig. 3b dominates, as expected. However, at higher μN , the one-to-five pathway became increasingly dominant (Supplementary Fig. 5a). The main reason for this is that the one-to-five pathway suppresses the stepping-stone pathway, and the strength of this suppression increases with the mutation rate. This happens because the two pathways start in the same way with a DD \rightarrow DS (or SD) transition (see Methods for two-letter strain nomenclature). However, while the DP mutant required to form a stable three-strain community gets to be evolutionarily favoured only towards the end of the transition, after sensitive individuals accumulate, the SD mutant required to initiate the one-to-five pathway is evolutionarily favoured straight away. As the population mutation rate is increased, it becomes increasingly likely that an SD mutant will arise before the point where DP mutants start to be selected for, and this will increasingly send the system along the one-to-five trajectory. Moreover, late-arising DP mutants do not inhibit the one-to-five pathway, but instead tend to stabilize it by prolonging the co-occurrence of DS and SD strains (Supplementary Fig. 4). As μN is increased and the one-to-five path-

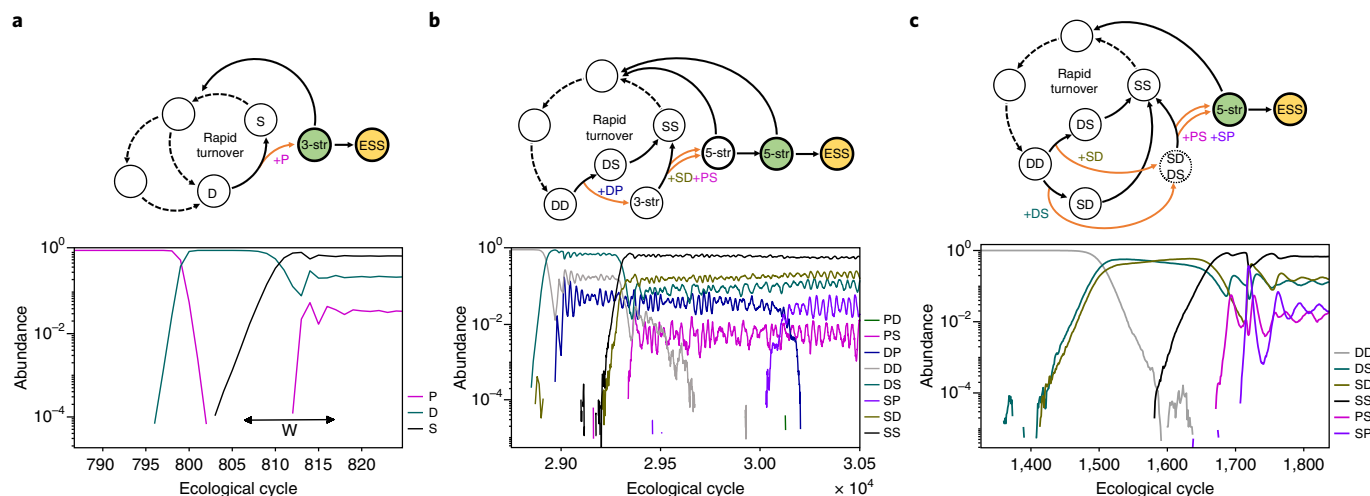


Fig. 3 | Pathways of ESC emergence. Sample simulation trajectories leading to multi-strain community formation (bottom) together with the corresponding state transition diagrams (top). Higher-order eco-evolutionary events are indicated as orange arrows. Communities of the same type as ESC (ESC-like; Methods) are shown in green. **a**, In simulations with one antibiotic, the strain turnover dynamics occasionally leads to a situation in which a resident degrader strain (D) is being outcompeted by a sensitive strain (S). As S increases in frequency, antibiotic producer strains (P) become evolutionarily favoured as well. However, if a producer strain arises too late, it will simply outcompete the sensitive strain. A producer must arise within a particular time window (W) for an ecologically stable three-strain (3-str) community to form, if such a community is possible at all, given the particular numerical values of the P and D phenotypes. **b**, One of the possible pathways for formation of a five-strain (5-str) community maintained by two antibiotics. The turnover dynamics leads to a state dominated by a strain that degrades both antibiotics (DD). While this strain is being outcompeted by a strain that degrades only the first antibiotic (DS), a DP strain arises and invades as well, leading to the formation of a three-strain (DP, DD and DS) ecologically stable community (see Methods for two-letter strain nomenclature). During the invasion of this community by a strain sensitive to both antibiotics (SS), two additional mutants (SD and PS) also invade, which leads to an ecologically stable five-strain community (after the loss of the DD strain). **c**, Another frequently utilized pathway for five-strain community formation. A DD strain is outcompeted by DS and SD strains. Through clonal interference, this two-strain community (dotted line circle) persists long enough for the SS strain to arise. As SS increases in frequency, antibiotic producer strains become selected for (SP and PS). If these strains arise before the extinction of DS or SD, an ecologically stable five-strain community can form.

ways starts to dominate, the initial stage of the pathway from DD to co-occurrence of DS, SD and SS strains experiences an efficient tunnel saturation, which drives the transition order to below four for the mutation rates examined (Supplementary Fig. 5b). This efficient saturation is brought about by the existence of pairs of DS and SD strains that are very close in fitness in the absence of other strains (Methods). Such ecologically distinct but nearly neutral pairs can persist for an extended time and effectively act as stepping-stone stable communities, which reduces the emergence order from five to four when the mutation rate is not too low.

Next, we sought to generalize our findings beyond the particular antibiotic interactions model used so far. To this end, we systematically investigated the different possible scenarios for the simplest order of tunnelling transitions—those from a one-strain to a three-strain community (Fig. 4). For each scenario, we present an argument for the functional form of $r(\mu, N)$, construct a simple ecological model that instantiates it and verify the functional form through computer simulations. We focus on three strains that can form an ecologically stable community, but for which all two-strain communities are unstable. We assume that strain 2 is in the process of outcompeting strain 1, and we determine the probability that an appearance of an individual of strain 3 will lead to the formation of the stable three-strain community.

Of central importance for the classification of the possible functional forms of $r(\mu, N)$ is the positioning of the basin of attraction of the three-strain community relative to the border line that corresponds to an adaptive transition from strain 1 to strain 2 in the absence of strain 3. The first possibility is that the basin of attraction intersects this border line (Fig. 4a). This is the scenario corresponding to the antibiotic interaction model and $r \sim (\mu N)^2$ scaling we have discussed so far (Supplementary Fig. 6). The duration of the exit

window W is independent of N for large N . Moreover, the probability that a single copy of strain 3 will escape stochastic loss is also asymptotically independent of N (Methods). A second possibility is that the basin of attraction extends all the way to the corner corresponding to strain 2 (Fig. 4b); corner 1 is less relevant, assuming selection against strain 3 there. In this case, an extra factor of $\log[N]$ has to be added to the community formation rate because the average time it takes for strain 2 to outcompete strain 1 exhibits $\log[N]$ dependence. This is provided that the selection coefficient (s_{21}) with which 2 outcompetes 1 is strictly positive and not arbitrarily close to zero for the entire transition (Methods and Supplementary Fig. 7). In contrast, if $s_{21} \rightarrow 0$ near a corner, the transition time will exhibit a stronger dependence on N . In particular, if $s_{12}(x_1) \rightarrow x_1^\alpha$ as $x_1 \rightarrow 0$ for some $\alpha > 0$, where x_1 is the relative abundance of strain 1, the transition time will scale as N^γ with $\gamma = \alpha/(1 + \alpha)$, and the overall community formation rate will be $r \sim (\mu N)^2 N^\gamma$ (Fig. 4c, Supplementary Fig. 8 and Methods).

The scaling relationships presented in Fig. 4b,c emerge from the behaviour of the dynamics near the corner of strain 2 and rely on the assumption that the rate of mutations generating strain 3 is not strongly dependent on the community composition. However, if strain 3 can only arise by mutation of strain 1, the extra N dependence of r would be reduced since the region where strain 2 dominates becomes less important for community formation. In particular, the scenarios from Fig. 4b,c with $\alpha < 1$ will lead to $r \sim (\mu N)^2$ at high N , and those from Fig. 4c with $\alpha = 1$ will lead to $r \sim (\mu N)^2 \log[N]$ (Supplementary Figs. 7e and 8e,f).

The final possibility for the basin of attraction (as determined in the limit of large N) is that it does not touch the border line (Fig. 4d). This scenario can exhibit different behaviours depending on the relative magnitude of the gap Δ and the population size

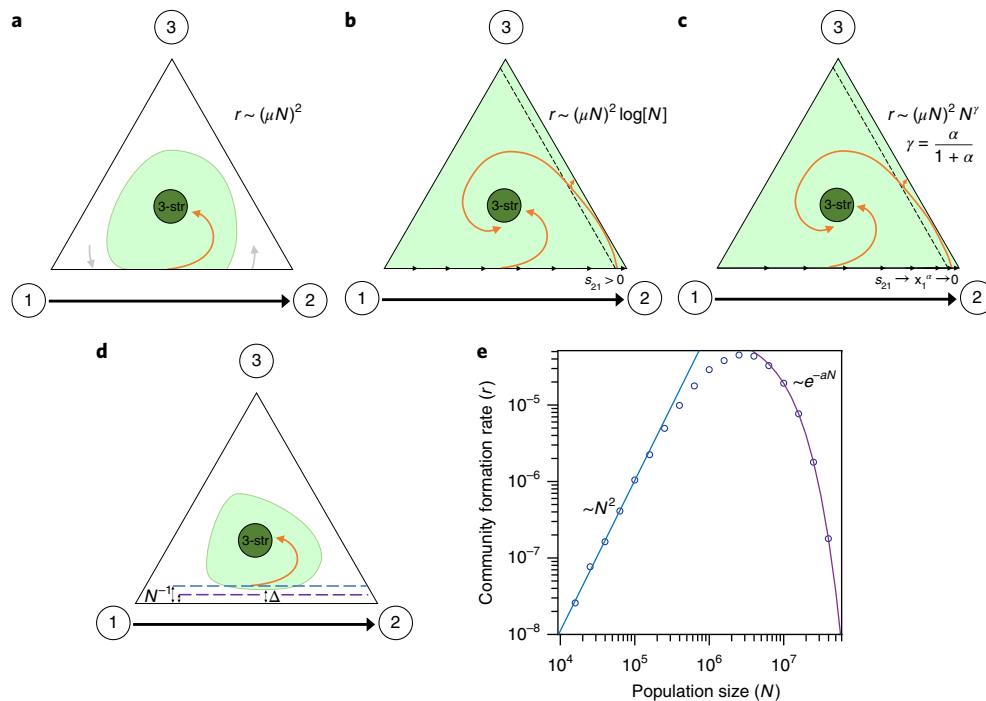


Fig. 4 | Different types of eco-evolutionary tunnelling transitions from one-strain to three-strain communities. $r(N)$ dependence is presented for qualitatively different cases. A community state is represented as a point within the triangle that specifies the relative strain abundances. The abundance of a strain is given by the distance to the edge opposite to its named vertex. The green shaded region is the basin of attraction of the fixed point corresponding to three-strain coexistence (dark green circle). An adaptive transition from strain 1 to strain 2 corresponds to a movement of the system state along the bottom side of the triangle. **a**, The basin of attraction covers a segment along the 1 → 2 transition. Strain 3 appearing along this segment and escaping stochastic loss will lead to formation of a three-strain community. The time it takes to traverse this segment and the escape probability are both asymptotically independent of N . **b**, The basin of attraction extends to corners 1 and 2, and the selection coefficient of strain 2 over strain 1 (s_{21}) is strictly positive. The time it takes to reach a boundary layer where stochastic loss of strain 1 becomes important (black dashed line) scales as $\log[N]$. This makes the probability that strain 3 emerges and leads to a three-strain community proportional to $(\mu N)\log[N]$. **c**, Similar to **b**, but strains 1 and 2 become asymptotically neutral as the abundance of strain 1 (x_1) approaches zero, so that the system spends a longer time near the corner of strain 2. This leads to N^γ ($\gamma < 1$) dependence of the transition time and r . **d**, There is a gap Δ between the basin of attraction and the line corresponding to absence of strain 3. For small N , a single member of strain 3 can put the system within the basin of attraction despite the gap (blue dashed line), leading to a situation similar to **a**. For $N > 1/\Delta$ (purple dashed line), the three-strain community is unreachable unless there is a lucky fluctuation of the ecological dynamics or additional mutations generating strain 3. **e**, Simulation data for the case presented in **d**, revealing an optimum population size for community formation. For $N < 1/\Delta$, r increases linearly with N^2 (blue fit). For $N > 1/\Delta$, r decreases exponentially with N (purple fit).

N (Fig. 4e and Supplementary Fig. 9). If $1/N > \Delta$, a single mutant individual of strain 3 can position the system within the basin of attraction. For small Δ , this would lead again to a regime of $r \sim (\mu N)^2$ scaling. If $1/N < \Delta$, community formation requires not only a timely emergence of strain 3, but also a lucky demographic fluctuation that pushes it into the basin of attraction. This leads to an exponential decrease of the community formation rate with N at fixed μ . Thus, strikingly, community formation is optimal at an intermediate population size of $N \approx 1/\Delta$. Interestingly, non-monotonic dependence of the tunnelling rate with N has previously been noted in the context of fitness-valley crossing, but the effect is reversed, with the tunnelling rate reaching a global minimum rather than maximum at intermediate values of $N^{37,43}$.

The classification presented in Fig. 4 applies to models with perfect mixing between ecological cycles, where the system state can be fully characterized by the abundances of the different strains. Analysis of models with spatial structure is more complicated because the probability of community formation depends on where a mutant lands within a spatially patterned community. We simulated the classic rock–paper–scissors model with spatial structure^{44,45} and empirically determined $r \sim (\mu N)^2 N^{0.5}$ (Supplementary Fig. 10 and Methods). Thus, spatially structured models can also exhibit power-law scaling of the community formation rate with μ and N .

We further explored the effect of spatial structure on the emergence of ESC in the context of our antibiotic interaction model. Instead of having one community that is well mixed at the end of every ecological cycle, we simulated communities connected by migration. We examined the rate of community formation (defined as the rate of first emergence of ESC at any location) as a function of the migration rate (Fig. 5a). The limit of low migration corresponds to many independent small communities, whereas very high migration corresponds to a single, large community that exhibits a higher rate of community emergence due to the non-trivial μN scaling. Strikingly though, community formation is fastest at intermediate migration rates, indicating that spatial structure facilitates eco-evolutionary emergence. A way to understand this is that, as migration rates are lowered from high to intermediate, a point is reached where the communities at different locations fail to synchronize their rapid turnover dynamics, and therefore immigration can introduce new strains into a community, effectively augmenting mutation.

Another spatial phenomenon we might expect from systems with a stable and metastable phase is that the stable phase will grow when in contact with the metastable one (Fig. 5b). This is known as nucleated growth⁴⁶. Therefore, we asked whether a small spatial region containing an ESC would expand and outcompete

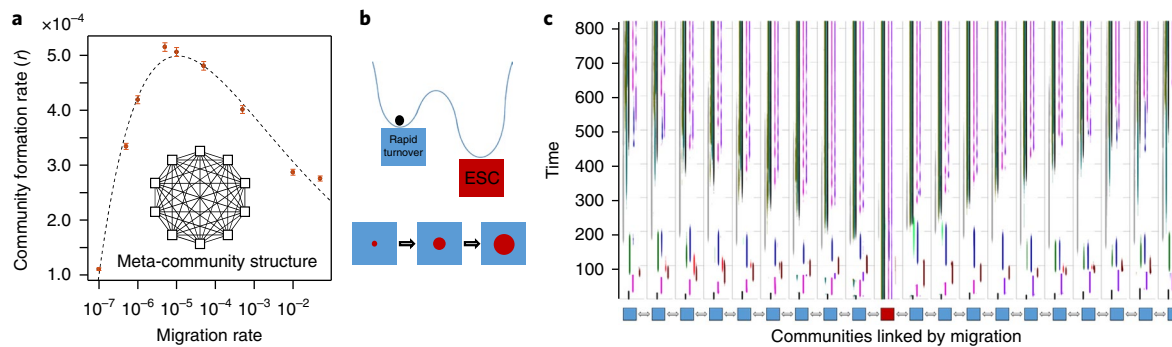


Fig. 5 | Accelerated emergence and spread of ESC in spatially extended systems. **a**, The community formation rate r is shown as a function of the migration rate for ten patches linked by migration. The rate is highest at intermediate migration rates. The error bars indicate 95% confidence intervals based on fitting the exponential distribution to the empirical distribution of community formation times. **b**, For systems with a stable (maroon) and metastable (blue) phase, nucleated growth is expected in which a (sufficiently large) seed of the stable phase grows and displaces the metastable phase. **c**, A one-dimensional chain of patches linked by migration is simulated in a universe with two antibiotics. The central patch is seeded with the five-strain ESC and the other patches contain a single strain sensitive to both antibiotics. Shown for each patch are the existing phenotypes as a function of time. The five-strain pattern corresponds to ESC spreads to neighbouring communities at an approximately constant speed, after an initial delay due to the special initial state of the non-central patches.

neighbouring communities. This is indeed what happens (Fig. 5c). This is significant because it constitutes an example of a multi-strain community that grows and spreads as a self-replicating unit. Thus, we have shown that eco-evolutionary tunnelling can lead to the spontaneous formation of composite, higher-level units of replication. The ability to spread implies that even if the emergence of a diverse community is unlikely at any given location, it only needs to arise once to become ecologically dominant.

Discussion

This work brings together two domains of evolutionary theory. On the one hand, it extends adaptive dynamics to the stochastic regime of finite mutation rates. On the other hand, it generalizes population genetics studies at finite mutation rates to the regime where different ecotypes can spontaneously emerge and reshape the fitness landscape. It has been previously appreciated that systems undergoing adaptive dynamics can either reach evolutionary equilibria or exhibit stochastic oscillations or chaos. At the same time, it has been shown within population genetics that populations can tunnel from one local fitness optimum to another in the presence of multiple mutations. The work presented here shows that populations can similarly tunnel between different attractors of the adaptive dynamics. Unlike tunnelling between fitness peaks, which requires deleterious mutations, the eco-evolutionary tunnelling described here can be driven entirely by positively selected mutants.

The formation of stable communities through a stochastic escape from a regime of rapid strain turnover via several well-timed mutant invasions is a mechanism for adaptive diversification that is fundamentally different from that relying on branching points. Its hallmarks—abrupt emergence without a complete set of stable intermediates, exponential distribution of the community formation time, superlinear scaling of the formation rate with population size, and colonization ability—are all experimentally testable, either directly from time-series data of individual trajectories (as illustrated by Fig. 3) or through replicate microcosm experiments.

This mechanism demonstrates that evolution of complex communities that is impossible as a series of independent evolutionary steps can nevertheless be efficient and generic in sufficiently large communities. It constitutes an example of an emergent phenomenon that is fundamentally eco-evolutionary. It is only possible when the timescales of the ecological and evolutionary dynamics overlap. The mutation rate per population is a parameter that controls this

overlap and can be viewed as a measure of evolutionary ‘temperature’, with adaptive dynamics being akin to a zero-temperature limit. In analogy with communities of atoms and molecules where numerous phenomena and phases of matter (for example, liquids) only exist at non-zero temperatures, we expect that there is a rich spectrum of eco-evolutionary phenomena and states that are only possible in the regime in which population mutation rates are not close to zero and multiple ecologically relevant invasions can be underway at the same time. We anticipate that further work will elucidate many additional such phenomena in both sexual and asexual populations. Our work might also have implications for economic theory where recent work has highlighted the difficulties of reaching complex Nash equilibria⁴⁷.

Methods

The computer simulations used in this study are based on the model described in ref. ⁴² and are briefly summarized in Fig. 1c–e. For the results presented in Fig. 4, the model was extended to include multiple patches linked by migration, as described below. All the simulations and numerical analyses were performed in MATLAB using custom scripts.

μ is the probability of mutation per individual per ecological cycle. N is the number of spores/individuals at the beginning of each ecological cycle and is kept constant by randomly sampling N spores at the end of the ecological cycle to start a new one. Mutations happen between ecological cycles, and the number of mutations that happen in the population between cycles is Poisson distributed with mean μN . The relative probabilities of different types of mutations are kept fixed when varying μ or N and are as described in the previous work.

Definition of ecological and evolutionary stability. Ecological stability is defined as the long-term persistence of diversity when mutations are turned off (despite demographic noise coming from finite population size). ESCs are ecologically stable communities for which no mutants exist that can increase in frequency and alter the community composition.

Classification of strains into discrete phenotypic classes. While phenotypes are continuous in simulations, we found it useful for analysis, visualization and interpretation of the results to assign them to several discrete categories. With respect to a single antibiotic, we distinguish D, S, R and P strains. A D strain is one that has the ability to degrade the antibiotic at some level. A P strain is a strain that produces the antibiotic at a level that can inhibit a neighbouring S strain colony. An R strain has an efflux pump making it resistant to the antibiotic (just as a P strain), but does not produce enough antibiotic to inhibit neighbours. The S strain does not degrade, produce or efflux antibiotics and is therefore sensitive to the antibiotic. In simulations with 2 antibiotics, we have 16 classes that correspond to all possible pairs of {D, S, R, P}. For example, a DP strain is a strain that can degrade the first antibiotic at some level and produce the second antibiotic at some level. In figures presenting evolutionary trajectories, strains from different phenotypic classes are shown in different colours, and strains from the same phenotypic class have the same colour.

ESC-like communities. In simulations, the true ESC is never reached as the selection coefficients of mutations that bring the community closer to ESC become vanishingly small, and the approach slows down. Furthermore, the gradual final approach to ESC proceeds through adaptive dynamics (selective sweeps within emergent ecotypes) and is not of primary interest. What we focus on is the transition from a population dominated by a single strain to an ecologically stable multi-strain community from which the evolution towards ESC can proceed entirely through adaptive dynamics. Correspondingly, we define the notion of an ESC-like community as an ecologically stable community that consists of strains that belong to the same phenotypic classes (see above) as the ESC.

In simulations with 1 antibiotic, ESCs consisted of three strains for the parameters we used: the S strain, a particular P strain and a particular D strain. An ESC-like community is therefore an ecologically stable community consisting of a P strain, a D strain and the S strain. In simulations with two antibiotics, ESC consists of five strains: particular PS, SP, DS and SD strains, and the SS strain. An ESC-like community is an ecologically stable community containing five strains that belong to these five phenotypic classes.

Determining the community formation time T . For each simulation, we determined the ecological cycle number (time) of the first occurrence (if any) of an ESC-like community. This was done algorithmically through the following heuristic procedure.

First, we determine the abundance over time for the ESC-like phenotypic classes. In simulations with one antibiotic, we keep track of the abundance of P, D and S phenotypic classes over time. For simulations with two antibiotics, we record the abundance of PS, SP, DS and SS classes over time. For example, the abundance of the SP class is determined by summing the abundances of all SP strains that exist at a particular time. Typically, the abundance was recorded every ten ecological cycles.

To determine whether an ESC-like community emerges at time point t , we analyse the phenotypic class abundance trajectories over the 6 subsequent time points (including the current time point), spanning 50 ecological cycles. If the abundance of any ESC-like phenotypic class reaches zero during this interval, time point t does not mark the onset of an ESC-like community. If all abundances stay positive, we compute the linear least-squares fits for each phenotypic class. We then calculate the relative slope of each linear fit by dividing the change in abundance by the maximum value over the time interval. If all the relative slopes (for the ESC-like phenotypes) are below 0.05, we mark t as the time of ESC-like community formation. For each simulation trajectory, the time of first emergence of an ESC-like community is taken to be the community formation time T .

The accuracy of this algorithm has been validated by manually examining thousands of evolutionary trajectories. The scaling of r with μN is insensitive to the time interval and threshold used, although they might lead to a shift of the distribution of T by a constant amount or a multiplicative shift of r (for example, due to rejection of very short-lived ESC-like communities).

Verifying that the community formation time is exponentially distributed and determining the community formation rate r . For particular values of μ and N , thousands of replicate trajectories lasting for tens of thousands of ecological cycles (see 'Parameters' for exact values) were generated (starting with different random-number generator seeds). For each trajectory, we determined the community formation time T . If no community formed, we set T to infinity.

We then constructed the empirical cumulative distribution function $CDF(t) = \text{Prob}(T < t)$, which specifies the fraction of trajectories with T smaller than t . If T is exponentially distributed, we expect $\text{Prob}(T \geq t) = 1 - CDF(t) = \exp(-rt)$, and correspondingly a linear relationship between $y = \log[1 - CDF(t)]$ and t . Strong linearity was indeed observed, as shown in Supplementary Figs. 1 and 2.

The slope provides an estimate of r . Note that the exponential distribution will, in general, be shifted due to the non-random initial condition and the finite duration of a higher-order eco-evolutionary event (see τ_0 below). Correspondingly, we allowed the fitted line not to pass through the origin ($y = -rt + a$).

Error bars for the community formation rates (r) were estimated as the standard 95% confidence interval for the slope coefficient of the linear regression between y and t .

Migration. A meta-community model of H patches is characterized by an $H \times H$ migration matrix M . M_{ij} specifies the fraction of the population from community j that migrates to community i in one ecological cycle.

We considered two spatial settings in this paper:

- (1) All-to-all connected patches (Fig. 4a), for which we set $M_{ij} = m(1 - \delta_{ij}) + (1 - (H-1)m)\delta_{ij}$, where δ_{ij} is the Kronecker delta symbol and m is the migration rate. $H = 10$ was used.
- (2) A ring of patches (Fig. 4c), implemented as $M_{ij} = (1 - 2m)\delta_{ij} + m(\delta_{i,j+1} + \delta_{i,j-1} + \delta_{i,H} \delta_{j,1} + \delta_{i,1} \delta_{j,H})$. The last two terms connect patches 1 and H to create a ring. $H = 20$ was used.

If $Y_{i,s}$ is the abundance of strain s in patch j at the end of an ecological cycle, we set $\tilde{Y}_{i,s} = \sum_{j=1}^H M_{ij} Y_{j,s}$ and start the next ecological cycle of patch i by randomly assigning strain phenotypes to N individuals according to a multinomial

distribution with $p_{i,s} = \tilde{Y}_{i,s} / \sum_s \tilde{Y}_{i,s}$. The ecological cycles of all patches are synchronous.

For the all-to-all connected meta-community, the overall community formation time was defined as the time when any of the communities reached an ESC-like state according to the algorithm described above.

The rate ($1/\langle T \rangle$) of reaching a state through adaptive dynamics is proportional to μN . Adaptive dynamics assumes that the system is mutation limited. The system spends almost all of its time waiting for the next successful mutant to invade and drive its transition from one ecological attractor to another. The waiting times at each state (circle in Fig. 1a,b) are exponentially distributed, and each possible transition (arrow in Fig. 1a,b) is characterized by a transition rate—the probability per unit time that the adaptive mutant underlying the specific transition will appear and escape stochastic loss. Each transition rate is therefore proportional to μN . If the rapid turnover dynamics is driven by mutant invasions with non-negligible selection coefficients, at low μN the transitions themselves will have negligible duration compared with the mean wait times. Correspondingly, the mean time it takes to hop along any particular sequence of state transitions is equal to the sum of mean waiting times for each hop along the trajectory. Therefore, the mean time to reach any state (ecological attractor) from any other is proportional to $(\mu N)^{-1}$ (as long as no nearly neutral transitions are required). Based on the observation that the turnover of strains is indeed rapid, it is clear that the turnover dynamics is pushed forward by mutants with non-negligible selection coefficients.

Rate of community emergence in simulations with one antibiotic. The basic idea is that the rapid turnover dynamics passes through exit windows. During such passes, there is some probability that a community will form through a higher-order eco-evolutionary event.

Let τ be the average time it takes the rapid turnover adaptive dynamics to return to an exit window, if currently at one. Based on the argument above, $\tau \sim (\mu N)^{-1}$ at low μN .

Let P be the probability that a community will form through a higher-order eco-evolutionary event during an ongoing passage through an exit window. In general, the dynamics will pass through an exit window many times before a community eventually forms successfully. For simplicity, let us imagine there is a single exit window, and let $n = 1, 2, 3, \dots$ be the number of times the dynamics passed through it before success. n is a geometrically distributed random variable, and $\langle n \rangle = 1/P$. Correspondingly, the mean community formation time is:

$$\langle T \rangle = (\langle n \rangle - 1)\tau + \tau_0 = \tau(1-P)/P + \tau_0,$$

where τ_0 is the sum of the mean time to reach the exit window from the initial condition and the mean time it takes for the community to come together after reaching the exit window for the last time.

As $P \rightarrow 0$, it follows that $\langle T \rangle \rightarrow \tau/P$ and therefore $r \rightarrow P/\tau$.

In the one-antibiotic case, escape from the rapid turnover regime requires a single well-timed mutant invasion; that is, a P strain must invade during an adaptive dynamic transition from an S strain-dominated community to a D strain-dominated community. The P strain must arise during some time window W ; if the P strain arises too late, it will take over the community dominated by the S strain. Let $q \sim \mu N$ be the probability per ecological cycle that such a mutant will arise and escape stochastic loss. Then, $P = 1 - (1 - q)^W \approx 1 - \exp(-qW)$. Therefore, $P \sim \mu N$ for small μN , and correspondingly, $r \sim (\mu N)^2$, provided that the duration of the time window W and the probability q are independent of N . This would be the case if the basin of attraction for the three-strain community is as shown in Fig. 4a (with D, S and P strains corresponding to strains 1, 2 and 3, respectively). In this scenario, a community can form only if strain 3 arises when $x_2 \in (a, b)$, where x_2 is the relative abundance of strain 2, and a and b are fixed values different from 0 and 1. As N is increased, the dynamics becomes more deterministic, and the time it takes to traverse the segment from a to b would converge to a finite value. At the same time, using the classical population genetics formula for the fixation probability, the probability that a strain 3 mutant arising at a particular point $x_2 \in (a, b)$ would escape stochastic loss converges to $\max(0, 2s_3(x_2))$ for large N , where $s_3(x_2)$ is the selection coefficient of a strain 3 mutant along the $1 \rightarrow 2$ transition. Thus, q would be asymptotically independent of N as well.

Note that if qW is not small, the approximation $P \sim \mu N$ no longer holds. Thus, as we increase μN , we would expect deviations from $r \sim (\mu N)^2$. If qW is of order unity, P can be close to 1 as well, and we might get $r \sim \mu N$. Thus, the scaling exponent of r can decrease at high enough μN . Deviations from power-law scaling are indeed noticeable at high μN in Fig. 2d.

Rate of community emergence in simulations with two antibiotics. Generalizing the logic from above, if k mutations need to arise during an ongoing adaptive dynamic transition for a community to emerge, this will lead to $P \sim (\mu N)^k$ for small μN .

The pathway presented in Fig. 3b can be split into two tunnelling transitions. First, a higher-order eco-evolutionary event is required to arrive at the three-strain (SD + DP + DD) ecologically stable community. Repeating the argument for one antibiotic, the rate of arriving at this three-strain community is $r_3 \sim (\mu N)^2$. The three-strain community can collapse following a mutant invasion

and can be considered a part of an extended strain-turnover loop. The formation of a five-strain community requires a second higher-order eco-evolutionary event to exit this extended loop. During an invasion of the three-strain community by a DS strain, two additional mutants (SS and SP) need to arise. Correspondingly, the probability of success is $P_{3 \rightarrow 5} \sim (\mu N)^2$. Repeating the logic from the one-antibiotic case, now with the extended turnover loop that incorporates the three-strain community, we get: $r = r_3 P_{3 \rightarrow 5}$, and therefore $r \sim (\mu N)^4$ at low μN .

For the pathway presented in Fig. 3c, four mutations need to arise during an ongoing transition from DD to, say, DS, which implies $P \sim (\mu N)^4$ and, using $r = P/\tau$, $r \sim (\mu N)^5$. This indeed might be the case at very low μN . However, starting from the lowest μN levels we could computationally explore, this was one of the main channels for the formation of five-strain communities (Supplementary Fig. 5), indicating a lower apparent scaling exponent. A qualitatively new feature of this pathway is the DS + SD two-strain intermediate. The relative selection coefficients of the DS and SD strains depend on the properties of the DD strain they derive and take over from. Each time the turnover dynamics reaches a DD, it will have a somewhat different phenotype. Crucially, some DD strains will give rise to DS and SD strains that have nearly identical selection coefficients. If this happens, DS and SD will coexist in a near-neutral fashion for extended periods of time (clonal interference), virtually guaranteeing that this two-strain combination will persist until a mutant invasion. Thus, DS + SD can effectively act as a regular ecologically stable community awaiting a mutant invasion. The five-strain community formation can then be viewed as a set of two higher-order eco-evolutionary events: the first creating the DS + SD state by means of an SD invasion during a DD to DS transition, and the second creating the five-strain community through PS and SP invasions during a DS + SD to SS transition. The rate of reaching SD + DS would be $(\mu N)^2$, as for the one-antibiotic case, and the probability of the second eco-evolutionary tunnelling is $(\mu N)^2$ because of the two required well-timed mutations. Therefore, we expect $r \sim (\mu N)^4$ for pathways with long-lived SD + DS states, which is of the same order as the pathway in Fig. 3b.

Alternative models without spatial structure. Simple models with three strains that can exhibit eco-evolutionary tunnels were constructed using the formalism of discrete replicator dynamics. Let x_1, x_2 and x_3 be the relative abundances of the three strains and $f_i(x_1, x_2, x_3)$, $i = 1, 2, 3$ be functions that specify their frequency-dependent fitness. Then, the discrete-time, stochastic, finite population size ecological dynamics is specified by:

- (1) setting $z_i(t) = \frac{f_i x_i(t)}{\sum_j f_j x_j(t)}$; (2) sampling N individuals from the multinomial

distribution specified by $\{z_1(t), z_2(t), z_3(t)\}$ to obtain the number of individuals, $X_i(t+1)$, from each strain; and (3) setting $x_i(t+1) = X_i(t+1)/N$. Evolutionary dynamics is added by randomly switching individuals from one strain to another with a probability μ per individual per generation.

The fitness functions used for Fig. 4b,c and their accompanying Supplementary Figs. 7 and 8 are of the form:

$$f_1 = 1 + ax_1^\alpha + bx_3^\alpha$$

$$f_2 = 1 + ax_2^\alpha + bx_1^\alpha$$

$$f_3 = 1 + ax_3^\alpha + bx_2^\alpha$$

where a, b and α are model parameters (see ‘Parameters’ section for Supplementary Figs. 7 and 8). $a > 0$ introduces an Allee effect (intra-strain cooperation). $a = 0$ leads to asymptotic neutrality near the corners of the two-simplex, as presented in Fig. 4c. The term proportional to b means that strains increase each other’s fitness in a cyclic fashion. $b > a$ ensures that no two strains can stably coexist.

The fitness functions used for the gapped model from Fig. 4d and Supplementary Fig. 9 are:

$$f_1 = R_1(1 + k_1 x_3^2 + k_2 x_1 x_3)$$

$$f_2 = R_2$$

$$f_3 = R_3(1 - 2x_1 x_3 - x_1^2)$$

This is a minimal model of ecological dynamics with antibiotic production and degradation, which is based on averaging the outcomes of all possible triplets of interacting strains. Strain 1 can be considered an antibiotic producer, strain 2 a degrader and strain 3 an antibiotic-sensitive strain. R_1, R_2, R_3, k_1 and k_2 are model parameters (see ‘Parameters’ section for Fig. 4e and Supplementary Fig. 9).

Spatial rock–paper–scissors model with evolution. A 2D rock–paper–scissors model without migration was set up as described in ref. 45. Briefly, a lattice point can belong to one of three strains, or be empty (four possible states). Each cell can

transition between states based on its four nearest neighbours. The transitions depend on two rates: μ for the reproduction rate and σ for the selection rate (as defined in ref. 45). The simulations were carried out as a discrete stochastic model on a 2D square lattice with periodic boundary conditions. We update the lattice at fixed time intervals (Δt). At each time step, the total rate (ρ_{ij}) of all possible pixel changes is calculated for each pixel with coordinates i and j . The probability of a change of a pixel during a time step is given by: $P_{ij} = 1 - e^{-\rho_{ij} \Delta t}$. All the pixel updates are independent. In addition, at each time interval, a pixel can randomly switch from one strain to another with probability m (not to be confused with the rate of reproduction, μ) per generation.

Community formation rate for alternative models without spatial structure. If P is the probability of community formation after the start of a transition from strain 1 to strain 2, and $T_{12}(N)$ is the average number of time steps the transition takes, we can express the community formation rate (at low μN) as:

$$r(\mu, N) \sim (\mu N) P = (\mu N) \{ \mu N T_{12}(N) \} P_{CF}(N) = (\mu N)^2 T_{12}(N) P_{CF}(N)$$

Here, $\mu N T_{12}(N)$ is proportional to the mean number of strain 3 mutants that are expected to arise during the transition, and $0 \leq P_{CF}(N) \leq 1$ is the probability that a single strain 3 mutant (at initial frequency $1/N$) arising at a random time during the transition will lead to community formation. Given the bounds on $P_{CF}(N)$, it is clear that as long as $P_{CF}^* = \lim_{N \rightarrow \infty} P_{CF}(N) > 0$ we would have $r \sim (\mu N)^2 T_{12}(N)$ for large N , which is indeed the behaviour we see in simulations (the case from Fig. 5a is an example corresponding to $P_{CF}^* = 0$). P_{CF}^* depends only on the system behaviour near $x_1 \rightarrow 0$ and $x_2 = 1 - x_1 \rightarrow 0$ since the transition spends almost all of its time there for large N (Supplementary Fig. 7c). For the models presented here, the $x_2 \rightarrow 0$ corner does not contribute because the probability of community forming starting with a strain 3 there is zero (Supplementary Fig. 7d).

Finding the functional form of $T_{12}(N)$ corresponds to the classical problem of calculating the mean fixation or loss time of a beneficial mutation⁴⁸. If the selection coefficient of strain 2 relative to strain 1, $s_{12}(x_1)$, is strictly positive and finite, we have $T_{12}(N) \sim \log[N]$ (Supplementary Fig. 7a). This can be understood based on a deterministic calculation. Assuming for simplicity that s_{12} is constant, we have $x_2(t)/x_1(t) = x_2(0)/x_1(0) \exp(s_{12}t)$. Therefore, the time it takes to transition from $x_2(0) = 1/N$ to $x_1(T_{12}) = 1/N$ exhibits $\log[N]$ dependence. However, if $s_{12}(x_1) \rightarrow (x_1)^\alpha$ as $x_1 \rightarrow 0$, then (for $\alpha > 0$) strains 1 and 2 become asymptotically neutral as strain 2 approaches fixation. This slows down the transition and leads to $T_{12}(N) \sim N^\gamma$, with $\gamma = \alpha/(1 + \alpha)$ (Supplementary Fig. 8). Thus, $\gamma \leq 1$, with $\gamma = 1$ corresponding to neutral dynamics.

Parameters. The parameters are defined in ref. 42. The 2D Gaussian filter used in all steps was size 5×5 and $\sigma = 1$. $\alpha = 0.5, \lambda = 0.5, \Gamma = 0.3, \delta = 2, T_p = 40, T_r = 10, N = 40, L = 100, S = 3,600, D_{\max} = 1,000, P_{\max} = 1,000, \mu = 10, \{\pi_{1D}, \pi_1, \pi_2\} = \{1/3, 1/3, 1/3\}, \epsilon = 0$.

Figure 1d. $C_D^0 = 0.03, C_D = 4 \times 10^{-4}, C_p = 4 \times 10^{-4}, C_R = 0.3, \mu N = 4, N = 1.44 \times 10^5$.

Figure 2a. $C_D^0 = 0.03, C_D = 4 \times 10^{-4}, C_p = 4 \times 10^{-4}, C_R = 0.3, \mu N = 0.25, N = 1.44 \times 10^5$.

Figure 2b. 1,000 replicate simulations with the following parameters: $C_D^0 = 0.06, C_D = 2 \times 10^{-4}, C_p = 8 \times 10^{-5}, C_R = 0.35, \mu N = 0.025, N = 1.44 \times 10^5$.

Figure 2d. **Simulations with one antibiotic.** $C_D^0 = 0.06, C_D = 8 \times 10^{-5}, C_p = 2 \times 10^{-4}, C_R = 0.35, N = 1.44 \times 10^5, \mu N = \{0.1, 0.0875, 0.075, 0.0625, 0.05, 0.0375, 0.025, 0.0125, 0.00875\}$. 1,000 replicate simulations per μN value. Each simulation was run until it reached an ESC-like state.

Simulations with two antibiotics. $C_D^0 = 0.06, C_D = 4 \times 10^{-5}, C_p = 8 \times 10^{-4}, C_R = 0.3, N = 1.44 \times 10^5$. 1,000 replicates per μN were run for 70,000 ecological cycles for $\mu N = \{0.8, 0.7, 0.6, 0.5, 0.4\}$. 1,000 replicates were run for 150,000 ecological cycles for $\mu N = 0.3$. 1,000 replicates were run for 50,000 ecological cycles for $\mu N = 0.2$. 1,000 replicates were run for 50,000 ecological cycles for $\mu N = 0.15$. 5,000 replicates were run for 160,000 ecological cycles for $\mu N = 0.1$. 10,000 replicates were run for 240,000 ecological cycles for $\mu N = 0.05$.

Figure 3a. $C_D^0 = 0.06, C_D = 8 \times 10^{-5}, C_p = 2 \times 10^{-4}, C_R = 0.35, N = 1.44 \times 10^5, \mu N = 0.05$.

Figure 3b. $C_D^0 = 0.06, C_D = 4 \times 10^{-5}, C_p = 8 \times 10^{-4}, C_p^0 = 0.3, N = 1.44 \times 10^5, \mu N = 0.4$.

Figure 3c. $C_D^0 = 0.06, C_D = 4 \times 10^{-5}, C_p = 8 \times 10^{-4}, C_R = 0.3, N = 1.44 \times 10^5, \mu N = 0.7$.

Figure 4e. $R_1 = 1.6, R_2 = 1.81, R_3 = 1.9, k_1 = 1.1, k_2 = 1, N = \{15,849, 25,119, 39,811, 63,096, 100,000, 158,489, 251,189, 398,107, 630,957, 1,000,000, 1,584,893, 2,511,886, 3,981,072, 6,309,573, 10,000,000, 15,848,932, 25,118,864, 39,810,717\}, T = 100,000$, number of replicates = 50,000. $\mu = 5 \times 10^{-8}$.

Figure 5a. Number of antibiotics = 1. $C_D^0 = 0.06, C_D = 8 \times 10^{-5}, C_p = 2 \times 10^{-4}, C_R = 0.35, N = 1.44 \times 10^5, \mu N = 0.05, m = \{0.05, 0.01, 5 \times 10^{-4}, 5 \times 10^{-5}, 1 \times 10^{-5}, 5 \times 10^{-6}, 1 \times 10^{-6}, 5 \times 10^{-7}, 1 \times 10^{-7}\}, H = 10$. 500 replicate simulations per μN . Each simulation was run until it reached an ESC-like state.

Figure 5c. Number of antibiotics = 2. $C_D^0 = 0.03$, $C_D = 4 \times 10^{-5}$, $C_p = 4 \times 10^{-4}$, $C_R = 0.30$, $N = 1.44 \times 10^5$, $\mu N = 2$, $m = 5 \times 10^{-5}$, $H = 20$.

Supplementary Fig. 1. Same as Fig. 2d.

Supplementary Fig. 2. Same as Fig. 2d.

Supplementary Fig. 3a. **Simulations with one antibiotic.** $C_D^0 = 0.06$, $C_D = 8 \times 10^{-5}$, $C_p = 2 \times 10^{-4}$, $C_R = 0.35$. $N = \{4.32 \times 10^5, 3.6 \times 10^5, 2.88 \times 10^5, 2.16 \times 10^5, 1.44 \times 10^5, 7.2 \times 10^4, 3.6 \times 10^4\}$, corresponding to $\mu N = \{0.1, 0.083, 0.0667, 0.05, 0.033, 0.01667, 0.00833\}$. 500 replicate simulations per μN were run until they reached an ESC-like state.

Simulations with two antibiotics. $C_D^0 = 0.06$, $C_D = 4 \times 10^{-5}$, $C_p = 8 \times 10^{-4}$, $C_R = 0.3$. $N = \{3.6 \times 10^5, 2.88 \times 10^5, 2.16 \times 10^5, 1.44 \times 10^5, 7.2 \times 10^4\}$, corresponding to $\mu N = \{1, 0.8, 0.6, 0.4, 0.2\}$. 1,000 replicate simulations per μN were run for 70,000 ecological cycles.

Supplementary Fig. 3b. **Simulations with one antibiotic.** $C_D^0 = 0.06$, $C_D = 8 \times 10^{-5}$, $C_p = 2 \times 10^{-4}$, $C_R = 0.35$, $N = 1.44 \times 10^5$, μN constant at 0.1 and $N = \{4.32 \times 10^5, 3.6 \times 10^5, 2.88 \times 10^5, 2.16 \times 10^5, 1.44 \times 10^5, 7.2 \times 10^4, 3.6 \times 10^4\}$. 1,000 replicate simulations per μN were run until they reached an ESC-like state.

Simulations with two antibiotics. $C_D^0 = 0.06$, $C_D = 4 \times 10^{-5}$, $C_p = 8 \times 10^{-4}$, $C_R = 0.3$, $\mu N = 0.5$ and $N = \{3.6 \times 10^5, 2.88 \times 10^5, 2.16 \times 10^5, 1.44 \times 10^5, 7.2 \times 10^4\}$. 1,000 replicate simulations per μN were run for 70,000 ecological cycles.

Supplementary Fig. 4. $C_D^0 = 0.06$, $C_D = 4 \times 10^{-5}$, $C_p = 8 \times 10^{-4}$, $C_R = 0.3$, $N = 1.44 \times 10^5$, $\mu N = 0.5$.

Supplementary Fig. 5a. $C_D^0 = 0.06$, $C_D = 4 \times 10^{-5}$, $C_p = 8 \times 10^{-4}$, $C_R = 0.3$, $N = 1.44 \times 10^5$. $\{137, 121, 154, 97\}$ trajectories leading to community formation were classified by visual inspection for $\mu N = \{0.8, 0.4, 0.2, 0.1\}$.

Supplementary Fig. 5b. The two degradation levels of the DD strain are $D_1 = 400 - \Delta D/2$ and $D_2 = 400 + \Delta D/2$.

Supplementary Fig. 6a. The degradation level of the D strain is 176.5524. The production level of the P strain is 576.4392.

Supplementary Fig. 6b. The degradation level of the D strain is 779.2114. The production level of the P strain is 375.3660. The rest of the parameters are the same as in Fig. 2d (simulations with one antibiotic).

Supplementary Fig. 7. $a = 0.1$, $b = 0.3$, $\alpha = 1$.

Supplementary Fig. 8. $a = 0$, $b = 0.3$, $\alpha = 0.5, 1, 1.5, 2$.

Supplementary Fig. 9a,b. $R_1 = 1.6$, $R_2 = 1.81$, $R_3 = 1.9$, $k_1 = 1.1$, $k_2 = 1$ $N = \{1 \times 10^5, 1 \times 10^6, 5 \times 10^6, 1 \times 10^7, 3 \times 10^7, 4.5 \times 10^7, 6 \times 10^7, 8 \times 10^7\}$, $T = 100,000$, replicates = 50,000. For each value of N , $\mu = \{5 \times 10^{-10}, 1.5 \times 10^{-9}, 3.5 \times 10^{-9}, 5 \times 10^{-9}, 1.5 \times 10^{-8}, 3.5 \times 10^{-8}, 5 \times 10^{-8}, 6.5 \times 10^{-8}, 8.5 \times 10^{-8}, 1 \times 10^{-7}, 1.15 \times 10^{-7}, 1.35 \times 10^{-7}, 1.5 \times 10^{-7}, 2 \times 10^{-7}, 2.5 \times 10^{-7}, 3 \times 10^{-7}, 3.5 \times 10^{-7}\}$.

Supplementary Fig. 9c. $R_1 = 1.2$, $R_2 = 1.7$, $R_3 = 1.9$, $k_1 = 2$, $k_2 = 0$, replicates = 10,000, $T = 300,000$, $N = \{10,000,000, 25,118,864, 63,095,734, 158,489,319, 398,107,171, 1,000,000,000, 2,511,886,432, 6,309,573,445\}$, $T = 100,000$, $\mu N = 5 \times 10^{-3}$.

Supplementary Fig. 10. $\mu = 1$, $\sigma = 1$, $\Delta t = 0.5$. $T = 250,000$, $m = \{8 \times 10^{-8}, 3.6 \times 10^{-8}, 2 \times 10^{-8}, 8.8 \times 10^{-9}, 5 \times 10^{-9}\}$, $N = \{2,500, 5,625, 10,000, 22,500, 40,000\}$.

Reporting Summary. Further information on research design is available in the Nature Research Reporting Summary linked to this article.

Code availability. The MATLAB scripts used are available from <https://doi.org/10.5281/zenodo.1325963>.

Data availability. The datasets generated during this study are available from <https://doi.org/10.5281/zenodo.1325963>.

Received: 21 February 2018; Accepted: 30 July 2018;
Published online: 21 September 2018

References

- Schoener, T. W. The newest synthesis: understanding the interplay of evolutionary and ecological dynamics. *Science* **331**, 426–429 (2011).
- Pelletier, E., Garant, D. & Hendry, A. P. Eco-evolutionary dynamics. *Phil. Trans. R. Soc. Lond. B* **364**, 1483–1489 (2009).
- Haloin, J. R. & Strauss, S. Y. Interplay between ecological communities and evolution. *Ann. NY Acad. Sci.* **1133**, 87–125 (2008).
- Weber, M. G., Wagner, C. E., Best, R. J., Harmon, L. J. & Matthews, B. Evolution in a community context: on integrating ecological interactions and macroevolution. *Trends Ecol. Evol.* **32**, 291–304 (2017).
- Post, D. M. & Palkovacs, E. P. Eco-evolutionary feedbacks in community and ecosystem ecology: interactions between the ecological theatre and the evolutionary play. *Phil. Trans. R. Soc. B* **364**, 1629–1640 (2009).
- Sanchez, A. & Gore, J. Feedback between population and evolutionary dynamics determines the fate of social microbial populations. *PLoS Biol.* **11**, e1001547 (2013).
- Rainey, P. B. & Travisano, M. Adaptive radiation in a heterogeneous environment. *Nature* **394**, 69–72 (1998).
- Gómez, P. & Buckley, A. Real-time microbial adaptive diversification in soil. *Ecol. Lett.* **16**, 650–655 (2013).
- Callahan, B. J., Fukami, T. & Fisher, D. S. Rapid evolution of adaptive niche construction in experimental microbial populations. *Evolution* **68**, 3307–3316 (2014).
- Koeppl, A. F. et al. Speedy speciation in a bacterial microcosm: new species can arise as frequently as adaptations within a species. *ISME J.* **7**, 1080–1091 (2013).
- Hiltunen, T., Virta, M. & Laine, A.-L. Antibiotic resistance in the wild: an eco-evolutionary perspective. *Phil. Trans. R. Soc. Lond. B* **372**, 20160039 (2017).
- Fischbach, M. A., Walsh, C. T. & Clardy, J. The evolution of gene collectives: how natural selection drives chemical innovation. *Proc. Natl Acad. Sci. USA* **105**, 4601–4608 (2008).
- Celiker, H. & Gore, J. Clustering in community structure across replicate ecosystems following a long-term bacterial evolution experiment. *Nat. Commun.* **5**, 4643 (2014).
- Cordero, O. X. & Polz, M. F. Explaining microbial genomic diversity in light of evolutionary ecology. *Nat. Rev. Microbiol.* **12**, 263–273 (2014).
- Stein, R. R. et al. Ecological modeling from time-series inference: insight into dynamics and stability of intestinal microbiota. *PLoS Comput. Biol.* **9**, e1003388 (2013).
- Coyte, K. Z., Schluter, J. & Foster, K. R. The ecology of the microbiome: networks, competition, and stability. *Science* **350**, 663–666 (2015).
- Friedman, J., Higgins, L. M. & Gore, J. Community structure follows simple assembly rules in microbial microcosms. *Nat. Ecol. Evol.* **1**, 0109 (2017).
- Yoshida, T., Jones, L. E., Ellner, S. P., Fussmann, G. F. & Hairston, N. G. Rapid evolution drives ecological dynamics in a predator–prey system. *Nature* **424**, 303–306 (2003).
- Lawrence, D. et al. Species interactions alter evolutionary responses to a novel environment. *PLoS Biol.* **10**, e1001330 (2012).
- Herron, M. D. & Doebeli, M. Parallel evolutionary dynamics of adaptive diversification in *Escherichia coli*. *PLoS Biol.* **11**, e1001490 (2013).
- Harrington, K. I. & Sanchez, A. Eco-evolutionary dynamics of complex social strategies in microbial communities. *Commun. Integr. Biol.* **7**, e28230 (2014).
- Good, B. H., McDonald, M. J., Barrick, J. E., Lenski, R. E. & Desai, M. M. The dynamics of molecular evolution over 60,000 generations. *Nature* **551**, 45–50 (2017).
- Maynard Smith, J. & Price, G. R. The logic of animal conflict. *Nature* **246**, 15–18 (1973).
- Maynard Smith, J. *Evolution and the Theory of Games* (Cambridge Univ. Press, Cambridge, 1982).
- Levin, S. A. & Muller-Landau, H. C. The emergence of diversity in plant communities. *C. R. Acad. Sci. III* **323**, 129–139 (2000).
- Conlin, P. L., Chandler, J. R. & Kerr, B. Games of life and death: antibiotic resistance and production through the lens of evolutionary game theory. *Curr. Opin. Microbiol.* **21**, 35–44 (2014).
- Boyd, R. & Lorberbaum, J. P. No pure strategy is evolutionarily stable in the repeated prisoner's dilemma game. *Nature* **327**, 58–59 (1987).
- Nowak, M. A. & Sigmund, K. Evolutionary dynamics of biological games. *Science* **303**, 793–799 (2004).
- Geritz, S. A. H., Kisdi, E., Meszina, G. & Metz, J. A. J. Evolutionarily singular strategies and the adaptive growth and branching of the evolutionary tree. *Evol. Ecol.* **12**, 35–57 (1998).
- Diekmann O. *A Beginner's Guide to Adaptive Dynamics* Mathematical Modelling of Population Dynamics Vol. 63 (ed. Rudnicki, R.) 47–86 (Banach Center Publications, Warsaw, 2004).
- Brännström, Johansson, J. & von Festerberg, N. The hitchhiker's guide to adaptive dynamics. *Games* **4**, 304–328 (2013).
- Nowak, M. An evolutionarily stable strategy may be inaccessible. *J. Theor. Biol.* **142**, 237–241 (1990).
- Boldin, B. & Diekmann, O. An extension of the classification of evolutionarily singular strategies in adaptive dynamics. *J. Math. Biol.* **69**, 905–940 (2013).
- Doebeli, M. *Adaptive Diversification (MPB-48)* (Princeton Univ. Press, Princeton, NJ, 2011).
- Gerrish, P. J. & Lenski, R. E. The fate of competing beneficial mutations in an asexual population. *Genetica* **102/103**, 127–144 (1998).

36. Hegreness, M., Shores, N., Hartl, D. & Kishony, R. An equivalence principle for the incorporation of favorable mutations in asexual populations. *Science* **311**, 1615–1617 (2006).
37. Iwasa, Y., Michor, F. & Nowak, M. A. Stochastic tunnels in evolutionary dynamics. *Genetics* **166**, 1571–1579 (2004).
38. Desai, M. M. & Fisher, D. S. Beneficial mutation selection balance and the effect of linkage on positive selection. *Genetics* **176**, 1759–1798 (2007).
39. Weissman, D. B., Desai, M. M., Fisher, D. S. & Feldman, M. W. The rate at which asexual populations cross fitness valleys. *Theor. Popul. Biol.* **75**, 286–300 (2009).
40. Weissman, D. B., Feldman, M. W. & Fisher, D. S. The rate of fitness-valley crossing in sexual populations. *Genetics* **186**, 1389–1410 (2010).
41. Martens, E. A. Kostadinov, R., Maley, C. C. & Hallatschek, O. Spatial structure increases the waiting time for cancer. *New J. Phys.* **13**, 115014 (2011).
42. Vetsigian, K. Diverse modes of eco-evolutionary dynamics in communities of antibiotic-producing microorganisms. *Nat. Ecol. Evol.* **1**, 0189 (2017).
43. Weinreich, D. M. & Chao, L. Rapid evolutionary escape by large populations from local fitness peaks is likely in nature. *Evolution* **59**, 1175–1182 (2005).
44. Kerr, B., Riley, M. A., Feldman, M. W. & Bohannan, B. J. M. Local dispersal promotes biodiversity in a real-life game of rock–paper–scissors. *Nature* **418**, 171–174 (2002).
45. Reichenbach, T., Mobilia, M. & Frey, E. Mobility promotes and jeopardizes biodiversity in rock–paper–scissors games. *Nature* **448**, 1046–1049 (2007).
46. Karthika, S., Radhakrishnan, T. K. & Kalaichelvi, P. A review of classical and nonclassical nucleation theories. *Cryst. Growth Des.* **16**, 6663–6681 (2016).
47. Babichenko, Y. & Rubinstein, A. Communication complexity of approximate Nash equilibria. In *Proc. 49th Annual ACM SIGACT Symposium on Theory of Computing (STOC 2017)* 878–889 (ACM Press, 2017).
48. Kimura, M. & Ohta, T. The average number of generations until fixation of a mutant gene in a finite population. *Genetics* **61**, 763–771 (1969).

Acknowledgements

This work was supported by the Simons Foundation, Targeted Grant in the Mathematical Modeling of Living Systems Award 342039 and National Science Foundation Grant DEB 1457518. This research was performed using the compute resources and assistance of the University of Wisconsin-Madison Center for High Throughput Computing in the Department of Computer Sciences. We thank S. A. Levin and D. Weissman for insightful discussions.

Author contributions

S.E.K. and K.V. designed the study, analysed the data, performed the simulations and wrote the manuscript.

Competing interests

The authors declare no competing interests.

Additional information

Supplementary information is available for this paper at <https://doi.org/10.1038/s41559-018-0655-7>.

Reprints and permissions information is available at www.nature.com/reprints.

Correspondence and requests for materials should be addressed to K.V.

Publisher's note: Springer Nature remains neutral with regard to jurisdictional claims in published maps and institutional affiliations.

Reporting Summary

Nature Research wishes to improve the reproducibility of the work that we publish. This form provides structure for consistency and transparency in reporting. For further information on Nature Research policies, see [Authors & Referees](#) and the [Editorial Policy Checklist](#).

Please do not complete any field with "not applicable" or n/a. Refer to the help text for what text to use if an item is not relevant to your study.

For final submission: please carefully check your responses for accuracy; you will not be able to make changes later.

Statistical parameters

When statistical analyses are reported, confirm that the following items are present in the relevant location (e.g. figure legend, table legend, main text, or Methods section).

n/a Confirmed

- | | | |
|-------------------------------------|-------------------------------------|---|
| <input type="checkbox"/> | <input checked="" type="checkbox"/> | The <u>exact sample size</u> (n) for each experimental group/condition, given as a discrete number and unit of measurement |
| <input type="checkbox"/> | <input checked="" type="checkbox"/> | An indication of whether measurements were taken from distinct samples or whether the same sample was measured repeatedly |
| <input checked="" type="checkbox"/> | <input type="checkbox"/> | The statistical test(s) used AND whether they are one- or two-sided
<i>Only common tests should be described solely by name; describe more complex techniques in the Methods section.</i> |
| <input checked="" type="checkbox"/> | <input type="checkbox"/> | A description of all covariates tested |
| <input type="checkbox"/> | <input checked="" type="checkbox"/> | A description of any assumptions or corrections, such as tests of normality and adjustment for multiple comparisons |
| <input type="checkbox"/> | <input checked="" type="checkbox"/> | A full description of the statistics including <u>central tendency</u> (e.g. means) or other basic estimates (e.g. regression coefficient) AND <u>variation</u> (e.g. standard deviation) or associated <u>estimates of uncertainty</u> (e.g. confidence intervals) |
| <input checked="" type="checkbox"/> | <input type="checkbox"/> | For null hypothesis testing, the test statistic (e.g. F , t , r) with confidence intervals, effect sizes, degrees of freedom and P value noted
<i>Give P values as exact values whenever suitable.</i> |
| <input checked="" type="checkbox"/> | <input type="checkbox"/> | For Bayesian analysis, information on the choice of priors and Markov chain Monte Carlo settings |
| <input checked="" type="checkbox"/> | <input type="checkbox"/> | For hierarchical and complex designs, identification of the appropriate level for tests and full reporting of outcomes |
| <input checked="" type="checkbox"/> | <input type="checkbox"/> | Estimates of effect sizes (e.g. Cohen's d , Pearson's r), indicating how they were calculated |
| <input type="checkbox"/> | <input checked="" type="checkbox"/> | Clearly defined error bars
<i>State explicitly what error bars represent (e.g. SD, SE, CI)</i> |

Our web collection on [statistics for biologists](#) may be useful.

Software and code

Policy information about [availability of computer code](#)

Data collection

Custom MATLAB scripts were used. <https://github.com/VetsigianLab/Eco-evolutionary-tunneling>

Data analysis

Custom MATLAB scripts were used. <https://github.com/VetsigianLab/Eco-evolutionary-tunneling>

For manuscripts utilizing custom algorithms or software that are central to the research but not yet described in published literature, software must be made available to editors/reviewers upon request. We strongly encourage code deposition in a community repository (e.g. GitHub). See the Nature Research [guidelines for submitting code & software](#) for further information.

Data

Policy information about [availability of data](#)

All manuscripts must include a [data availability statement](#). This statement should provide the following information, where applicable:

- Accession codes, unique identifiers, or web links for publicly available datasets
- A list of figures that have associated raw data
- A description of any restrictions on data availability

The authors declare that the data supporting the findings of this work are available within the manuscript and its supplementary information.

Field-specific reporting

Please select the best fit for your research. If you are not sure, read the appropriate sections before making your selection.

Life sciences Behavioural & social sciences Ecological, evolutionary & environmental sciences

For a reference copy of the document with all sections, see [nature.com/authors/policies/ReportingSummary-flat.pdf](https://www.nature.com/authors/policies/ReportingSummary-flat.pdf)

Ecological, evolutionary & environmental sciences study design

All studies must disclose on these points even when the disclosure is negative.

Study description	The evolutionary process leading to complex stable communities of antibiotic producing and degrading bacteria was characterized. The study was conducted via multi-scale simulations implemented in MATLAB.
Research sample	For each set of parameters multiple replicate simulations of eco-evolutionary dynamics were carried out.
Sampling strategy	Data were generated in-silico with one the order of 1000 samples for each data point. For almost all data points the number of replicate simulations was enough to make the expected statistical errors for the community formation rates (the main statistical output) smaller than the symbol size used in the graphical presentation of data (~3% error).
Data collection	Evolutionary trajectories were generated with custom MATLAB scripts and the abundance of every strain was recorded over time.
Timing and spatial scale	The simulated environment is a 2D surface, consisting of 40 grids of size 100x100. Simulations were run for 10000-260000 feast-and-famine ecological cycles.
Data exclusions	No simulation data were excluded from the analyses. All replicate simulations were taken into account.
Reproducibility	All the data was generated by computer simulations. Therefore reproducibility is not an issue.
Randomization	Randomization was ensured by starting each simulation with a different seed for the pseudo-random number generator.
Blinding	The data analyses were algorithmic rather than manual, which ensured uniform treatment.
Did the study involve field work?	<input type="checkbox"/> Yes <input checked="" type="checkbox"/> No

Reporting for specific materials, systems and methods

We require information from authors about some types of materials, experimental systems and methods used in many studies. Here, indicate whether each material, system or method listed is relevant to your study. If you are not sure if a list item applies to your research, read the appropriate section before selecting a response.

Materials & experimental systems

n/a	Involvement in the study
<input checked="" type="checkbox"/>	<input type="checkbox"/> Unique biological materials
<input checked="" type="checkbox"/>	<input type="checkbox"/> Antibodies
<input checked="" type="checkbox"/>	<input type="checkbox"/> Eukaryotic cell lines
<input checked="" type="checkbox"/>	<input type="checkbox"/> Palaeontology
<input checked="" type="checkbox"/>	<input type="checkbox"/> Animals and other organisms
<input checked="" type="checkbox"/>	<input type="checkbox"/> Human research participants

Methods

n/a	Involvement in the study
<input checked="" type="checkbox"/>	<input type="checkbox"/> ChIP-seq
<input checked="" type="checkbox"/>	<input type="checkbox"/> Flow cytometry
<input checked="" type="checkbox"/>	<input type="checkbox"/> MRI-based neuroimaging